

Sea ice type maps from Alaska Synthetic Aperture Radar Facility imagery: An assessment

Florence M. Fetterer

Remote Sensing Applications Branch, Naval Research Laboratory, Stennis Space Center, Mississippi

Denise Gineris

Sverdrup Technology, Stennis Space Center, Mississippi

Ronald Kwok

Jet Propulsion Laboratory, California Institute of Technology, Pasadena

Abstract. Synthetic aperture radar (SAR) imagery received at the Alaska SAR Facility is routinely and automatically classified on the Geophysical Processor System (GPS) to create ice type maps. We evaluated the wintertime performance of the GPS classification algorithm by comparing ice type percentages from supervised classification with percentages from the algorithm. The RMS difference for multiyear ice is about 6%, while the inconsistency in supervised classification is about 3%. The algorithm separates first-year from multiyear ice well, although it sometimes fails to correctly classify new ice and open water owing to the wide distribution of backscatter for these classes. Our results imply a high degree of accuracy and consistency in the growing archive of multiyear and first-year ice distribution maps. These results have implications for heat and mass balance studies which are furthered by the ability to accurately characterize ice type distributions over a large part of the Arctic.

1. Introduction

On July 17, 1991, the European Space Agency's ERS 1 satellite was launched into a near-polar, sun-synchronous orbit from French Guiana. ERS 1 carries the first synthetic aperture radar (SAR) in space since the Seasat mission in 1978. ERS 1 data from receiving and processing stations around the world are being used for geophysical and operational applications as diverse as soil moisture monitoring and ocean wave spectra determination [European Space Agency, 1993]. Of particular interest to the polar research community are data from the Alaska SAR Facility (ASF) in Fairbanks. Both airborne and Seasat SAR data had amply demonstrated, prior to the launch of ERS 1, the utility of SAR for detailed and accurate information on ice motion and type. This information has been used in process studies (see, for example, *Fily and Rothrock* [1990]) and for practical applications, such as routing ships through ice-infested waters. The surety of useful polar geophysical information from SAR led to the establishment at the University of Alaska of a facility for processing and distributing SAR data [Carsey *et al.*, 1987]. From the outset it was decided that ASF should provide scientists with not only image data but also with geophysical products. These products, which are created on the Geophysical Processor System (GPS), are ice motion vectors, images of ice type (ice type maps), gridded ice type concentrations, and wave spectra. Key considerations in this decision were the efficacy of a central processing and distribution point for products, the maturity of the algorithms which would produce them, and the role these

products can potentially play in meeting the science objectives held by users of ASF data [Alaska SAR Facility Prelaunch Science Working Team, 1989]. Broadly, these objectives are to observe ice circulation, to verify and improve dynamic models of ice properties, to estimate fluxes of heat, mass, and momentum, to improve formulations of the constitutive laws of ice rheology, and to observe and explain changes in ice morphology [Carsey, 1989]. Observing the distribution of ice type in the Arctic supports and, in some cases, is crucial to the accomplishment of these objectives. For instance, validating the formulation of constitutive laws with observations requires that estimates of ice type be accurate and consistent to within a few percent. Ice type must often serve as a proxy for ice thickness, since thickness data are sparse. Ice type is therefore an important variable in flux calculations. Furthermore, if understanding the role of the Arctic in global climate change is a goal, then monitoring changes in the distribution of ice types and open water is essential owing to the feedback mechanism between ice extent and heat transfer [Rothrock and Thomas, 1990; Gloerson and Campbell, 1991].

The ice type algorithm in place on the GPS is a backscatter-based Bayesian maximum likelihood algorithm meant to run indiscriminately on SAR scenes within its spatial and temporal domain. Such a classifier is useful largely because it can generate ice type statistics in quantities much greater than could be produced by manual inspection or supervised classification of images. At present, over 5700 SAR images have been classified on the GPS and reside in the ASF product archive. If it is accurate, the algorithm substantially improves our ability to characterize ice type distributions over a large section of the Arctic. To assess the performance of the algorithm, we have compared ice type percentages

Copyright 1994 by the American Geophysical Union.

Paper number 94JC01911.
0148-0227/94/94JC-01911\$05.00

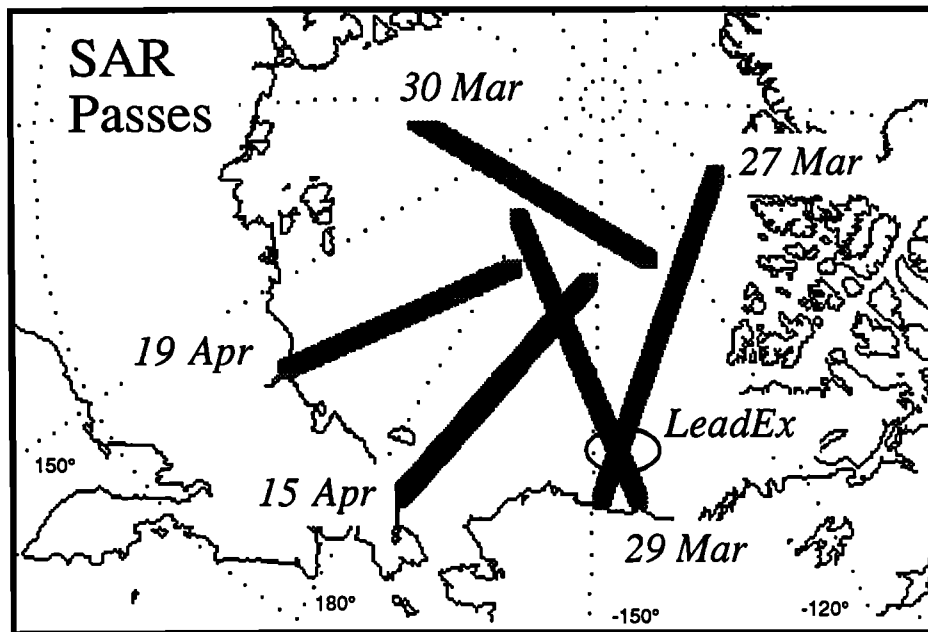


Figure 1. Approximately every other 100-km² image along each swath shown was selected for analysis. The location of the LeadEx experiment, which took place in March and April 1992, is indicated.

from the algorithm with ice type percentages from supervised classification on an image by image basis. We begin by describing the SAR data set used in the comparison. This is followed by a section describing the algorithm (and two variations which were also evaluated), as well as the expected backscatter distributions of ice types in ERS 1 imagery. The methodology of supervised classification and its limitations as a means of assessing accuracy are also discussed. In section 5 the results of the analysis are presented as statistics describing the accuracy of the classifier in terms of deviation from supervised classification. The algorithm assumes relatively stable and separable backscatter distributions for ice type classes. Errors caused by distribution variability and overlap are discussed in section 6. The concluding section remarks on the uncertain conformity between ice type labels and physical ice types or ice thickness, emphasizes what we believe to be the excellent separation of multiyear (MY) and first-year (FY) ice by the algorithm, and suggests areas for future work which may lead to algorithm improvement.

2. SAR Data Description

2.1. ERS 1 Image Data Characteristics

All image data used in this study are ERS 1 data collected within the ASF station mask and processed at ASF. The GPS uses calibrated, low-resolution images, which have a pixel spacing of 100 m and a nominal resolution of 240 m. Because low-resolution images are created by averaging full (30 m) resolution images, speckle in low-resolution images is insignificant. The calibrated images are a measure of the backscatter cross section of the imaged surface. Normalized backscatter cross section or σ^0 is the ratio of the radiance of radar energy reflected back toward the source to that incident on the surface per unit area. Backscatter depends on properties of the imaged surface, such as roughness and dielectric constant. ("Surface" here means the imaged ma-

terial. Backscatter can be due to surface scattering, volume scattering, or both.) Because surface roughness and dielectric properties vary with ice type, calibrated images can be classified on the basis of backscatter.

ASF imagery has an expected absolute and relative calibration accuracy of 2 dB and 1 dB, respectively [Fatland and Freeman, 1992]. Absolute calibration quantifies the uncertainty of a σ^0 measurement relative to the actual σ^0 of a surface. Typically, this appears as a bias when an identical surface area from two image frames (imaged at different times) are compared. Relative calibration measures how the backscatter of a surface known to have uniform backscatter appears to vary within an image. Relative calibration is usually better than absolute calibration and is easily maintainable, especially if the radar sensor is stable. The design of the classifier is such that it can accommodate errors in absolute calibration more readily than errors in relative calibration. The calibration accuracy and the noise equivalent σ^0 provide the sensor's limits to the discrimination of surface types by backscatter. The noise equivalent σ^0 of the ERS 1 radar data is at approximately -24 dB, which means that the backscatter from a surface with a σ^0 of -24 dB is equivalent to the noise power of the sensor. Surfaces with a backscatter cross section of less than -24 dB therefore, such as grease ice and perhaps some forms of new and young ice, have backscatter cross sections low enough to be below the noise floor of the sensor and are not easily detected. The backscatter of FY and MY ice is well within the dynamic range of the sensor.

2.2. The Image Data Set

The data set of 68 images selected for this study spans a period of approximately 3 weeks from March 28 to April 20, 1992. Geographically, the images sample the area between the Canadian Archipelago and the East Siberian Sea from 68°N to 84°N (Figure 1). Here we focus on the performance of the classifier under winter conditions, when the air

Table 1. ERS 1 Synthetic Aperture Radar Image Sea Ice Lookup Table for Winter

Ice Type	Mean Backscatter, dB	Standard Deviation, dB
MY	-10.0	1.01
FYR	-14.0	1.06
FYS	-17.0	1.26
NI/OW	-21.8	1.66

MY is multiyear; FYR, first-year rough; FYS, first-year smooth; and NI/OW, new ice or open water. See text for further ice type descriptions.

temperatures near the surface are below -10°C and where there is typically a dry snow cover over the sea ice with an absence of free water to modulate the backscatter signatures. The air temperature at the center location of each of the images was extracted from 1000-mbar National Meteorological Center analyzed fields. The temperature averaged about -20°C for all images. Under these relatively static conditions (in terms of sea ice backscatter) we can better examine the winter performance of the classifier.

3. The Classification Algorithm

The development of the algorithm in place at ASF has been reported by *Kwok et al.* [1992] and by *Cunningham et al.* [1992]. The following briefly describes the ASF algorithm and two additional versions.

3.1. Winter Lookup Table Description

The classification algorithm uses lookup tables containing parametric descriptions of the backscatter statistics of different sea ice types. There is a lookup table (LUT) for each season, since backscatter is affected by seasonal environmental conditions. The winter lookup table (Table 1) is used when temperatures are below -10°C . In the Beaufort Sea this is generally from October to mid-April. The winter LUT has entries for the four following ice types: MY ice, two types of FY ice, and an ice type with relatively low backscatter close to the system noise limit. One type of FY ice is considered to be rougher and more deformed. This type, termed first-year rough (FYR), has relatively high backscatter. A second FY type, termed first-year smooth (FYS), has lower backscatter, which may be due to a smoother surface. The final ice type is probably representative of new or young ice with low backscatter or of open water under calm conditions. It is labeled new ice or open water (NI/OW).

The names of the FY classes, which imply that the classes correspond to smooth and rough surfaces, may be misleading. When speaking of radar backscatter, "rough" generally means that the small-scale surface height variations are large compared with the radar wavelength. In this limited sense, then, rough FY ice will have a backscatter that is different from smooth FY ice, with the amount of difference depending on incidence angle. However, the 240-m resolution of the SAR data means that large-scale roughness features, such as ridges and hummocks, also contribute to pixel intensity, obscuring any straightforward relationship between roughness and backscatter. Even if one could assume homogeneous large- and small-scale roughness over the spatial scale of a SAR pixel, factors besides roughness which affect the

dielectric properties of the ice (such as salinity) can play a large part in determining the backscatter of FY ice. "Rough" and "smooth," then, can only refer to the characteristics of FY ice in an image as subjectively determined by the image analyst and as discussed in section 4.

The LUT was originally constructed using scatterometer measurements [*Kwok et al.*, 1992], rather than SAR measurements of backscatter. This is because it was not clear how to effectively assign backscatter distributions to ice types based on the limited amount of appropriate SAR data available before ERS 1. When ERS 1 imagery became available, the LUT backscatter statistics were refined. One reason for the difference between SAR and scatterometer-derived ice type backscatter statistics is that a SAR resolution element covers a much larger area than that of a surface scatterometer measurement. Therefore SAR pixels may contain a mixture of subtypes which can be distinguished in scatterometer data but are not resolved in SAR data. The LUT entries were corrected using backscatter samples from manually identified ice types in a small set of images from the winter of 1991. Subsequent work [*Kwok and Cunningham* 1994] and this study) has shown the corrected LUT values for MY ice to be stable and representative.

MY ice is readily separated from FY ice because the mean backscatter of MY ice differs from that of FY ice by several standard deviations. The discrimination of the various types of FY and younger ice is more difficult (as we shall illustrate) owing to the variability of their signatures, especially when ice is less than about a meter thick. Indeed, we do not attempt in this paper to associate each of these ice types with an expected thickness distribution. That task requires the compilation of extensive in situ measurements. Rather, the objective of this study is to evaluate the consistency of the backscatter of the ice types when those types are assigned by an operator. By doing so, we show the ability of automated classification to match the results of much more labor-intensive manual classification.

3.2. Maximum Likelihood Classification

Maximum likelihood, optimal, or Bayesian classification theoretically minimizes the probability of classifying an image pixel erroneously if the backscatter distributions of the different ice type classes are known. Formally, it is classification according to Bayes rule,

$$P(w_j|\mathbf{x}) = P(\mathbf{x}|w_j)P(w_j)/P(\mathbf{x})$$

which states that the a posteriori probability that a pixel with backscatter value \mathbf{x} is a member of class w_j ($P(w_j|\mathbf{x})$) is equal to the state conditional probability density function for \mathbf{x} or the likelihood of w_j with respect to \mathbf{x} ($P(\mathbf{x}|w_j)$) times the a priori probability of class w_j (or $P(w_j)$), divided by a normalization factor. Choosing the class for which $P(w_j|\mathbf{x})$ is greatest minimizes the probability of error [*Duda and Hart*, 1973].

For a one-dimensional feature vector, such as backscatter, evaluating $P(w_j|\mathbf{x})$ is conceptually simple. Figure 2 shows probability density functions (i.e., backscatter distributions) from the LUT for MY and FYR ice (solid line). There is overlap between the two classes, but the probability of choosing the wrong class is minimized by placing the decision boundary at \mathbf{x} where $P(\mathbf{x}|FYR) = P(\mathbf{x}|MY)$. ML classification assumes that the class distributions are normal. Note

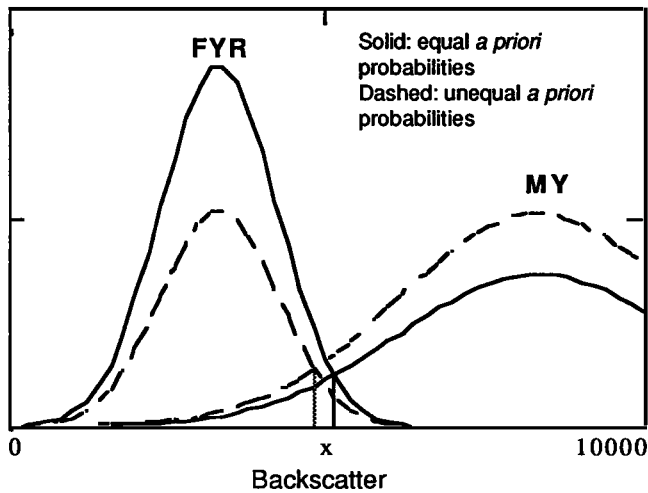


Figure 2. The probability density functions for first-year rough (FYR) and multiyear (MY) ice ($P(x|FYR)$, $P(x|MY)$) based on the lookup table (LUT) distributions. The dashed lines are density functions weighted by 70% probability of occurrence of MY ice, 30% probability for FYR ice. The horizontal axis is in units of intensity divided by a scale factor of 1.2×10^{-5} .

that backscatter is in units of intensity, rather than decibels. Both supervised and unsupervised classification takes place using the intensity (rather than decibels) represented by each pixel value after the image has been calibrated and corrected

for noise. Plate 1 shows a classification product for an image from about 72°N . MY ice appears to be readily distinguishable from FY and younger types. The algorithm has classified much of the first year ice as FYS. Some dark ice is classed as new ice or open water, although a sequence of images for this area over several weeks, as well as the bright linear features running through the area (these are presumed to be ridges), suggest that this ice is FY ice.

3.3. Maximum a Posteriori Classification

If a priori probabilities of occurrence are well known, then overall error can theoretically be reduced further. The dashed line in Figure 2 shows the probability density functions weighted by 70% for MY ice and 30% for FY ice. Note that the decision boundary shifts to the left, and more backscatter values are therefore classified as MY ice. If it is important to find most occurrences of a relatively rare class (such as new or FY ice in the Beaufort in winter), then it may not be desirable to use unequal or realistic prior probabilities, since doing so will reduce the number of cases correctly identified as the rare class. There is a trade-off between the detection of a class with a low probability of occurrence (for example, open water in the winter perennial ice zone) and the overall error for all the classes. Versions of the algorithm which use both equal and unequal prior probabilities were tested. The version which uses equal prior probabilities bases classification only on the probability density functions of the classes and is hereafter termed simply the maximum likelihood (ML) algorithm. The maximum a posteriori

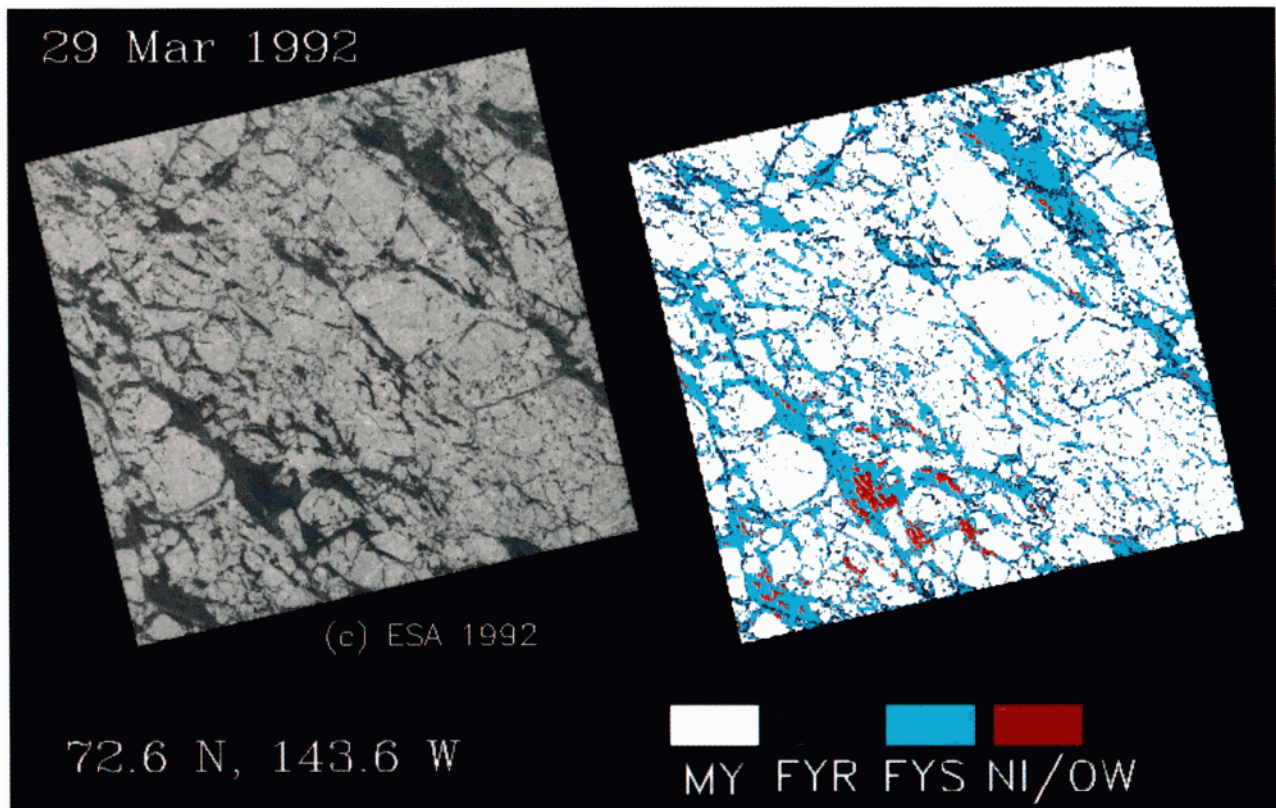


Plate 1. An ERS 1 synthetic aperture radar (SAR) image from the Beaufort Sea at approximately 72°N , with the algorithm-produced classification map. The algorithm found 67% multiyear (MY) ice, 16% first-year rough (FYR) ice, 15% first-year smooth (FYS) ice, and 2% new ice or open water (NI/OW). Copyright ESA 1992.

(MAP) version, on the other hand, first classifies the image using ML classification. On a second pass it reclassifies the image using, for the MY prior probability, the concentration of MY ice obtained from the first pass. The prior probabilities for the other classes are divided equally. This version is only applied when the initial classification results in MY concentration of 50% or greater, since not enough is known regarding the stability of the backscatter distributions of younger ice types in ERS 1 imagery to confidently assign prior probabilities to them on the basis of the initial classification. Of the 68 images used in this study, 52 had an initial MY ice concentration of greater than 50%. Considerations to using prior probabilities with maximum likelihood classification are given by *Strahler* [1980].

3.4. Estimating MY Backscatter

How well the algorithm does, of course, depends on how well the class distributions in an image have been approximated by the LUT. To account for shifts in overall image brightness caused by inaccurate calibration or other factors, the LUT is shifted relative to the mean backscatter of MY ice in the image being classified. (If no MY ice is identified, then the canonical LUT of Table 1 is used without modification.) The mean backscatter of MY ice is estimated from the image using an Isodata clustering routine. Isodata is an efficient form of maximum likelihood parameter estimation [*Duda and Hart*, 1973]. The backscatter cluster closest to the LUT value for MY ice is chosen as the MY cluster. Only a small (5%) portion of the image is clustered, which leads to an uncertainty in the estimate of mean MY backscatter of about 0.5 dB. (In addition, there is some uncertainty in the Isodata estimation procedure itself. MY ice is the standard because the backscatter of MY ice is relatively stable. Furthermore, the separation between MY and FY backscatter clusters is much greater than that between the other types, which allows a more accurate estimation of mean backscatter in Isodata). A 0.5-dB error in correctly identifying the mean backscatter of MY ice in an image leads to a 5–10% error in classification [*Kwok et al.*, 1992]. Therefore our benchmark for successful algorithm performance is absolute accuracy (accuracy independent of concentration) to within 10%.

3.5. Iterative Classification

Because uncertainty in the location of the mean backscatter for MY ice is a source of variability and error in classification, a third version of the algorithm obtains a more accurate estimate of mean MY backscatter by reclustering, in a second iteration, all those pixels classed as MY in the first iteration. This version is termed the ML iterative version. If results of the first pass are inaccurate, then the estimate of mean MY backscatter could potentially be worsened owing to the influence of misclassified pixels in the Isodata clustering routine. Results show that the improvement in parameter estimation due to the larger MY sample size more than offsets this potential error. Like MAP, this version is only applied when the initial classification results in MY concentration of 50% or greater. The ML iterative version has replaced the original ML version of the algorithm on the GPS at ASF.

4. Supervised Classification

Classifier performance was tested by comparing results from the three variations of the unsupervised maximum

likelihood algorithm with the result of supervised ML classification for each image. This method was chosen in order to provide a statistically large number of data points for comparison. To perform the standard manual classification of outlining individual ice types and totaling their area in each image would have been extremely time consuming, given the large number (68) of images used in the analysis and the large area covered by each image. As the supervised results are playing the important role of a substitute for surface observations in this analysis, it is necessary to thoroughly describe how they were obtained.

For every image analyzed a human interpreter selected a group of training areas from the image which were considered to be representative of the ice types present in the image. On average, two to four training areas were selected per ice type. With the exceptions noted below these ice types matched those of the LUT. Not all ice types were present in each image. The average size of the training areas depended somewhat on ice type. The majority of the images consisted of large floes of MY ice surrounded by and intermixed with smaller areas of first-year ice. Generally, the average training area sizes for MY, FYR, FYS, and NI/OW were 130 km², 20 km², 35 km², and 4 km², respectively. The minimum training area size was about 2 km² (or about 400 pixels). Uniformity was the key to training area selection. An attempt was made to select training areas from a variety of locations in the image. Generally, the ice type training areas selected easily correlated with one of the four ice type categories of the standard LUT. MY ice areas selected were free of isolated dark areas (which may be large frozen melt ponds or small areas of FY ice), frozen leads, or other features which would bias the statistics of the training area. The selected NI/OW training areas were completely featureless. FYS training areas were dark in appearance and featureless except for occasional well-defined ridges. FYR training areas were always brighter than FYS areas, had less contrast between features and background, and often appeared to be without defined ridges. The interpretation of this difference in appearance is that FYR ice generally has higher ridge density than FYS ice. A greater number of deformed features within each 100-m pixel raises overall brightness. Contrast is reduced because less background ice is undeformed.

Occasionally, rogue ice types or wind-roughened open water areas were encountered, and when the area of these “outliers” was large enough to be satisfactorily sampled, they were distinguished as separate surface types. Rough open water areas, found in four images, had high backscatter values of about –7 dB to –5 dB. Two MY ice subsets, bright MY ice (with a mean of –8.3 dB) and dark MY ice (with a mean of –12.2 dB), could be distinguished in a few images, and the concentrations of these ice types were summed with that of “normal” MY ice to form a total supervised MY ice concentration. Extremely bright (–6 dB) and small MY ice areas were found in two images, and the area covered by these patches was summed with that of normal MY ice. (These small patches of what we assume to be MY ice persist over at least several weeks in the study data set and in other examples from the larger Beaufort/Chukchi Sea winter data set.) The rough open water and extremely bright MY ice constituted only very small areas (<1%) of the imagery.

Once the training areas were established, lookup tables were formed for each image and ML classification was

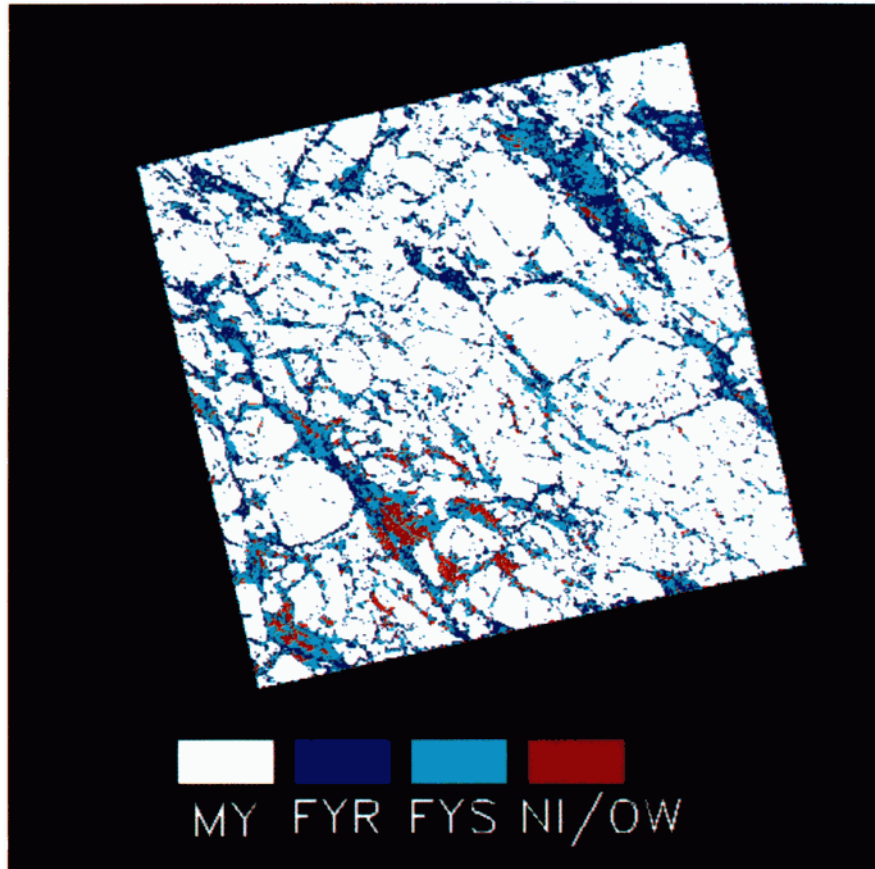


Plate 2. Supervised classification of the image shown in Plate 1. The analysis resulted in 72% MY, 16% FYR, 8% FYS, and 3% NI/OW.

performed on the calibrated images using the image-specific lookup tables. An example of supervised classification is presented in Plate 2. The supervised classification results were then compared to unsupervised classifications results. Note that while the percentage of MY ice is about the same for the supervised results in Plate 2 as for the algorithm results in Plate 1, the analyst found somewhat less of the FYS type.

Both supervised and unsupervised ML classification results in some error when overlap between classes exists. For instance, an analyst classifying MY and FY ice in an image in a completely manual fashion would include the pixels of a bright ridged area running through FY ice as part of the FY floe. Classification on the basis of backscatter, however, regardless of how carefully training sets are selected, would include the ridge pixels in the MY class. What we are assessing, then, is primarily the error in classification which comes from the mismatch between the calculated ice type backscatter distributions in the lookup table and the actual ice type backscatter distributions of the images. This error is minimized in supervised classification by the manual determination of lookup tables directly from the images. In addition, error due to subjectivity in the supervised results was minimized by having a single analyst perform the classifications over as short a time period as possible. A consistency check was performed on results from supervised classification by reclassifying several images after an extended period of time had passed. The supervised concen-

trations were recalculated and compared to the previous estimates. The change in estimated concentration was found to be 2.8%, 2.5%, 1.5%, and 1.9% for MY, FYR, FYS, and NI/OW, respectively. This indicates a large degree of stability in the measurements.

The discrepancy between what would be the results of completely manual analysis and supervised classification is probably largest for the NI/OW class. In some images, newly frozen leads provided the NI/OW training set. Much of the smooth FY ice was dark enough, however, to be included in this class, leading to an overestimation of the percentage of NI/OW by both supervised and unsupervised classification (see Plates 1 and 2). The classifier's performance in identifying the NI/OW class was not evaluated because there were not enough samples of this class in the imagery and because those samples that did exist had concentrations that were too small for a rigorous comparison to be performed (the concentration in all images except one was less than 10%, which is within the expected error of the algorithm). However, the signature of ice in freezing leads can overlap that of all other classes, depending on the stage of ice development and whether or not the thin ice has undergone deformation. In the case of open water the signature depends upon wind strength and other variables. Therefore neither supervised nor unsupervised algorithm classification will be able to properly identify this class except for cases where new ice is uniformly dark (not roughened by frost flowers or deformation) or where the wind speed is below a threshold of

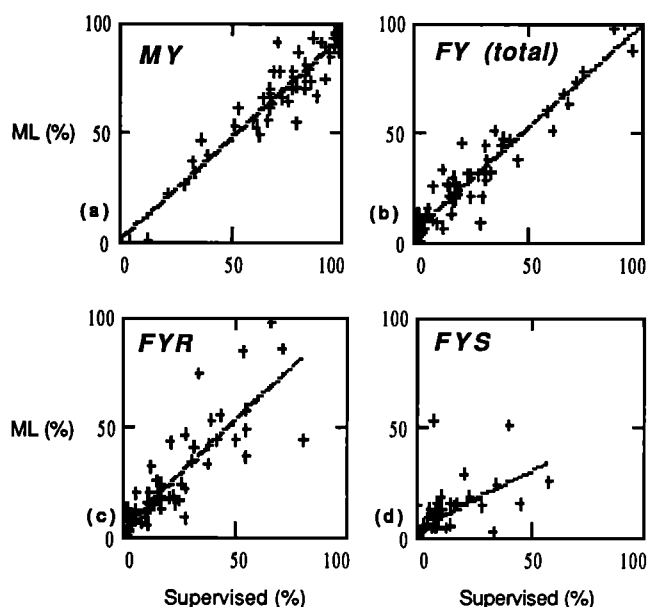


Figure 3. Percent concentration from supervised classification versus maximum likelihood (ML) algorithm concentration for (a) MY ice, (b) combined FY ice (FYR plus FYS), (c) FYR, and (d) FYS. Regression lines are also plotted.

approximately $3\text{--}5\text{ m s}^{-1}$. Results from the Lead Experiment (LeadEx) and other field experiments indicate that freezing ice in leads undergoes an evolution in backscatter with a range of the order of 10 dB over a period of hours [Onstott, 1992].

A database of ice backscatter signatures was formed from the training areas. The database consists of one table of data for each of the following major ice types: MY, FYR, FYS, and NI/OW. The tables contain 180, 95, 88, and 42 samples, respectively. For each training area the mean backscatter value of the area, standard deviation of the backscatter value, incidence angle to the area, and latitude and longitude of the area were tabulated, so that trends in the data could be examined. A lookup table was generated from this database for comparison with the standard LUT.

5. Comparison Results

Scattergrams of ML algorithm concentrations plotted against supervised concentrations with best fit regression lines are shown in Figure 3. Each point represents the concentration of an ice type in a single 100-km square image. Results for ML iterative and MAP are similar to those in Figure 3 (identical for cases where the concentration of MY is below 50%), with differences we will note presently. Theoretically, the regression lines in Figure 3 should be arrived at in a manner which assumes error in x as well as in y . For convenience, however, we will assume no error in x (the difference in the regression line would be small). Statistics describing error for each algorithm version in terms of fit to the regression line and the difference between algorithm and supervised concentrations are given in Table 2. Note that the agreement between ML and supervised classification is quite good for MY ice, with variance in the supervised value explaining 94% of the variance in the algorithm results. There is a slight positive bias, with supervised classification finding, on average, about 4% more MY ice. The RMS difference (our primary measurement for error) of 7.3% is only slightly (4.5%) higher than the estimated error (or inconsistency) in supervised classification. Marginally better results are obtained with the ML iterative version. The mean difference between algorithm and supervised results is reduced to 1%. The MAP version, on the other hand, merely biases the ML or ML iterative results by finding more MY ice owing to a more heavily weighted MY probability density function. If prior probabilities were added to the supervised classifier, then the MAP results would compare very well with supervised results. Prior probabilities are only useful to the extent that the probability density functions (i.e., backscatter distributions) are uncertain. Probability density functions are fairly certain for MY and FYR ice.

Figure 3b shows results for all FY ice (FYR and FYS combined). Because most images had very little new ice or open water, Figure 3b appears as the inverse of Figure 3a. The error statistics in Table 2 reflect this. Again, the ML iterative version performs best, with RMS error of only 6%. Figures 3c and 3d show the results for FYR and FYS, respectively. Here the agreement between supervised and algorithm results is poor. One reason for this is that the

Table 2. Difference Statistics for Algorithm Versus Supervised Classification

Ice Type	Algorithm Type	Regression Slope	Regression Intercept, %	R^2	Mean Difference, %	Standard Deviation Difference, %	RMS Difference, %
MY	ML	0.94	0.6	0.94	3.8	7.4	7.3
	iterative ML	0.96	1.5	0.95	1.0	6.1	6.2
	MAP	1.02	1.7	0.95	-3.3	7.2	7.3
All FY	ML	0.94	5.9	0.93	-4.2	7.4	7.3
	iterative ML	0.97	2.4	0.96	-1.5	5.9	6.0
	MAP	1.02	-3.7	0.95	2.8	7.0	7.0
FYR	ML	0.98	4.5	0.73	-4.0	11.4	11.5
	iterative ML	0.99	1.9	0.75	-1.7	10.7	11.1
	MAP	1.07	-3.9	0.75	2.6	11.9	12.0
FYS	ML	0.53	4.0	0.38	-0.2	10.1	8.5
	iterative ML	0.54	3.5	0.39	0.2	10.0	8.4
	MAP	0.54	3.5	0.39	0.2	10.0	8.4

Ice type abbreviations are same as in Table 1, and FY is first-year ice. R is the correlation coefficient from the regression, a measure of goodness of fit. ML is maximum likelihood; MAP, maximum a posteriori.

terms “deformed” or “rough” and “undeformed” or “smooth” FY ice are subjective. The analyst attempted to identify two classes of FY ice in each image. Sometimes two classes were not obvious. In those cases where only one type of FY ice could be observed a judgment was made based on brightness and general appearance as to which type of FY ice the case matched, and the ice was classified accordingly. Such cases usually occurred at higher latitudes where the size of FY floes tended to be smaller. For those cases where the single ice type could not be easily categorized it was classified as FYR ice (these cases were excluded from the compilation of FYR class statistics). Since the analyst was basing the decision to call FY ice deformed or undeformed on factors in addition to brightness, such as a large concentration of apparent ridges, relatively poor agreement with algorithm classification is not surprising. If error as a percentage proportional to concentration is considered, then the gulf between the good agreement for MY/FY separation and poor agreement for FYR/FYS separation widens.

Excluded from the data set in Figure 3 and Table 2 are outlying results from six images. In two of these images, FY ice in the fast ice shear zone north of Alaska was classified as MY ice. The remainder of the images were of areas of FY ice in the Chukchi Sea at about 69°N, which, probably because of its history in the seasonal ice zone, has a bright signature of -12 dB or higher. This ice is misclassified as MY by the algorithm, as shown in Plate 3a. These errors are predictable based on geographical region. For this reason, the proper domain of the algorithm is north of 73°. Our results show that while products south of 73° should be inspected for accuracy, the algorithm performs well in the central Arctic, East Siberian, Beaufort, and Chukchi Seas. No dependency of error on latitude is evident when residuals are plotted. However, several of the northernmost images were determined to be close to 100% MY ice by supervised classification. The algorithm finds about 8% FYR ice in these images (see Plate 3b). This is because pixels at the low end of the MY backscatter distribution are classed as FYR by the algorithm. Because the FY and MY LUT distributions overlap, the algorithm will erroneously find FY ice when only MY is present, unless all MY pixels are above the decision threshold of approximately -12 dB. As illustrated by Plate 3b, MY ice at latitudes between 75° and 80°N tends to have somewhat lower backscatter than MY ice farther south in this data set. *Kwok and Cunningham* [1994] verified the existence of an area of low backscatter at about this latitude in a much larger data set collected during the winters of 1991–1992 and 1992–1993. A possible explanation is that the lower backscatter may be due to higher fractional coverage of frozen melt ponds, while areas of higher backscatter, such as at higher and lower latitudes in our data set, are related to more intense deformation.

To summarize, the ML iterative algorithm in place at ASF produces results which are accurate to within 3% of the error inherent in this method of evaluation (about 3%) when separating MY from FY ice. The inclusion of prior probabilities does not improve classification accuracy. Although results are not presented here, all versions of the algorithm outperformed a minimum distance algorithm. (Minimum distance classification does not make use of class probability density functions.) The algorithm was less successful at separating two FY classes. The performance for the NI/OW

class was not evaluated owing to the small number of samples. However, it is clear from several examples that ice in freezing leads can exhibit a range of backscatter signatures which overlaps all classes and that wind-roughened water is classified as MY ice by the algorithm because of its high backscatter.

6. Classification Error and Backscatter Variability

6.1. Within- and Between-Class Variability

Obvious sources of classification error are between-class and within-class variability in the types being labeled. It is instructive therefore to ask what is the natural variability in the backscatter of FY and MY ice and how can it be expected to contribute to misclassification. A snapshot of backscatter variability from the study data set is shown in Figure 4. Each data point is the mean and standard deviation in backscatter from a single training set used in supervised classification. The distributions (by ice type) of the training set backscatter samples meet the chi-square test criterion for normality at a 95% confidence level. If this were not true, then the maximum likelihood algorithm would not be appropriate. Table 3 gives the mean and standard deviation of the data points in Figure 4. Normal distributions based on the means and standard deviations from the sample backscatter column in Table 3 constitute what we will call the found ice type distributions (in contrast to the LUT distributions). For MY ice the mean backscatter is slightly below the LUT value of -10 dB, while the mean backscatter for FYR is slightly higher than the LUT value. Variability in the mean of FY ice is greater than that of MY ice. While Figure 4 clearly shows the large overlap in backscatter between FYR and FYS ice, the mean values for FYR and FYS in Table 3 have nearly the same mean values and 3-dB separation between class means as in the LUT. This indicates that the LUT values are appropriate, if appropriateness is judged by agreement, on average, with the judgment of a human interpreter.

The theoretical error in ML classification caused by between-class and within-class variation is plotted in Figure 5. In Figure 5a, error (expressed as the sum of $P(\text{MY}|\text{FY})$ and $P(\text{FY}|\text{MY})$, see Figure 2) rises as the difference between the class mean for MY (or FY) ice and the LUT value for that mean increases in a negative (or positive) direction. At a difference of 0 the error level shows what the probability of overall error is if the separation of mean backscatter between MY and FY in the image is exactly equal to the LUT separation of 4 dB (and the standard deviations of the distributions match those in the LUT). When the means are closer by 1 standard deviation of the mean backscatter for MY ice from the training set (1 dB, see Table 3), the sum probability of error rises from 10% to 26%. Parenthetically, this plot also represents change in the probability of error due to inaccurately locating the mean MY backscatter during the Isodata clustering routine.

A similar analysis (Figure 5b) shows the probability of overall error due to within-class variation. Here error rises as the width of the actual FYR backscatter distribution in an image increases relative to the LUT FYR standard deviation. At a difference equivalent to 1 standard deviation (0.3 dB) in the standard deviation of FY backscatter from the

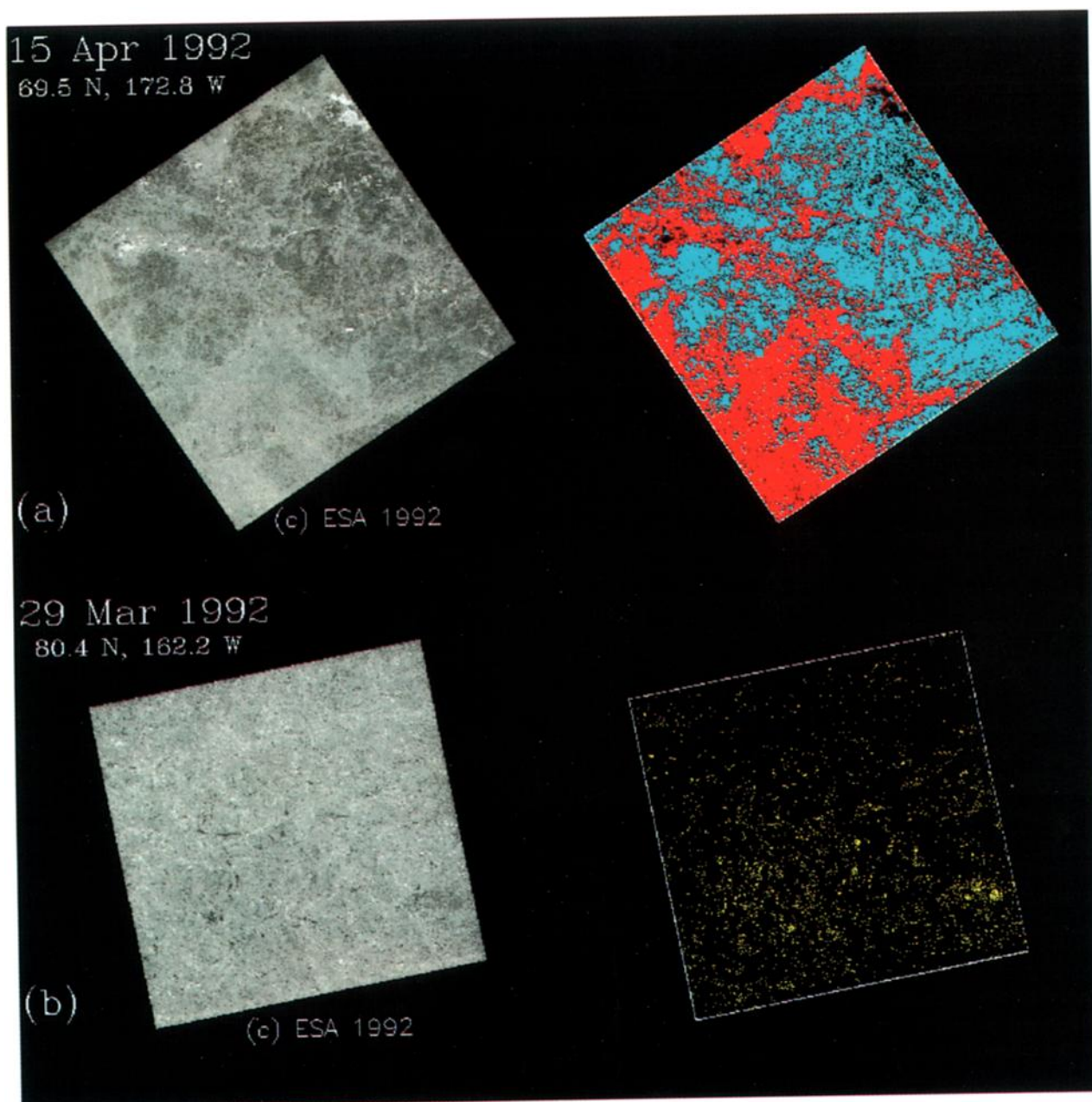


Plate 3. (a) Image (left) and classification error (right) for seasonal ice in the Chukchi Sea. This FY ice has a backscatter signature of about -12 dB, which causes much of it to be erroneously classified as MY ice by the algorithm. The red area is where supervised classification finds FYR and the algorithm finds MY, the cyan area is where supervised classification finds FYS and the algorithm finds FYR, and the black area is where both methods agree. (b) Image (left) and classification error (right) of MY ice at about 80° N. The analyst found 2% FY ice, while the algorithm found 8% (see text). The backscatter of MY ice in this image is about -11.6 dB with a standard deviation of 1.3 dB, or somewhat lower with a broader distribution than MY ice farther south. The yellow areas are where supervised classification finds MY, while algorithm classification finds FYR. The black area shows where both methods agree. Copyright ESA 1992.

training areas the sum probability of error rises from 10% to 13%.

Of course, if a change in the mean backscatter for a class is accompanied by a matching change in the other classes, there is no net effect on classifier results. This is because the algorithm has a sliding scale feature in which the LUT is shifted relative to the mean backscatter of MY ice in the image. Figure 6 shows the mean backscatter and the stan-

dard deviation of backscatter in decibels as a function of latitude. (The horizontal lines on the plots mark the LUT values. If the plots showed intensity, rather than dB, then the data points would be more evenly distributed around the horizontal lines.) Note that the backscatter of MY ice dips at about 77° N. That of FY ice exhibits a similar trend. However, further analysis showed that the relationship between FY and MY backscatter is only weakly linear for sample

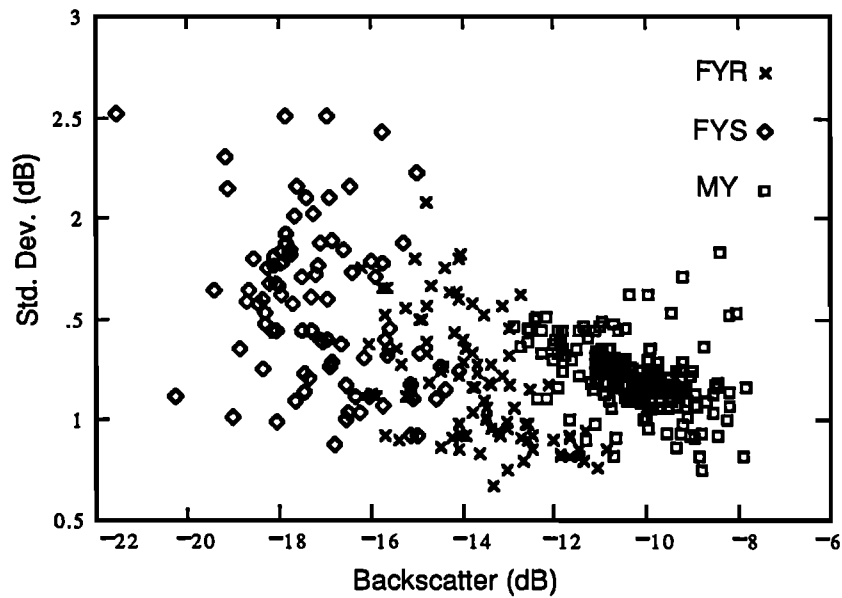


Figure 4. Mean and standard deviation of backscatter for each MY and FY training area in the data set. The downward trend in the plotted standard deviations is a result of weighting the standard deviation in intensity by the inverse of the mean backscatter value in order to express standard deviation in decibels.

means and not at all linear for sample standard deviations. Shifts in the mean backscatter of MY and FY ice are therefore only weakly correlated in this data set.

The sliding scale feature of the algorithm will improve classification accuracy for some images, but it does not have an effect on overall accuracy in this data set. The LUT distributions are plotted in Figure 7, as are the found distributions. The third trace in Figure 7 is of the LUT which would be applied (on average) to the data or, in other words, the LUT after an average shift of 0.2 dB to the left (since the mean found value for MY is -10.2, rather than -10 dB). Because the mean found backscatter for FYR ice is 0.4 dB higher than in the LUT, the shift would appear to worsen classification results. However, the distributions for any single image might look quite different from the found or average distributions, so it is better to assess potential error through regression analysis. Comparing the distributions in Figure 7 with the results of the regression analysis in Table 2 does show, though, that substitution of the found distributions for the LUT distributions would not yield an improvement in results.

Table 3. Mean and Standard Deviation of the Training Set Sample Means and Sample Standard Deviations for the Backscatter Samples Shown in Figure 4

Ice Type	Sample Backscatter		Sample Standard Deviation	
	Mean, dB	Standard Deviation, dB	Mean, dB	Standard Deviation, dB
MY	-10.2	1.0	1.2	0.3
FYR	-13.6	1.1	1.2	0.3
FYS	-17.0	1.2	1.5	0.6

Ice type abbreviations are same as in Table 1. Statistics are computed in intensity and converted to decibels.

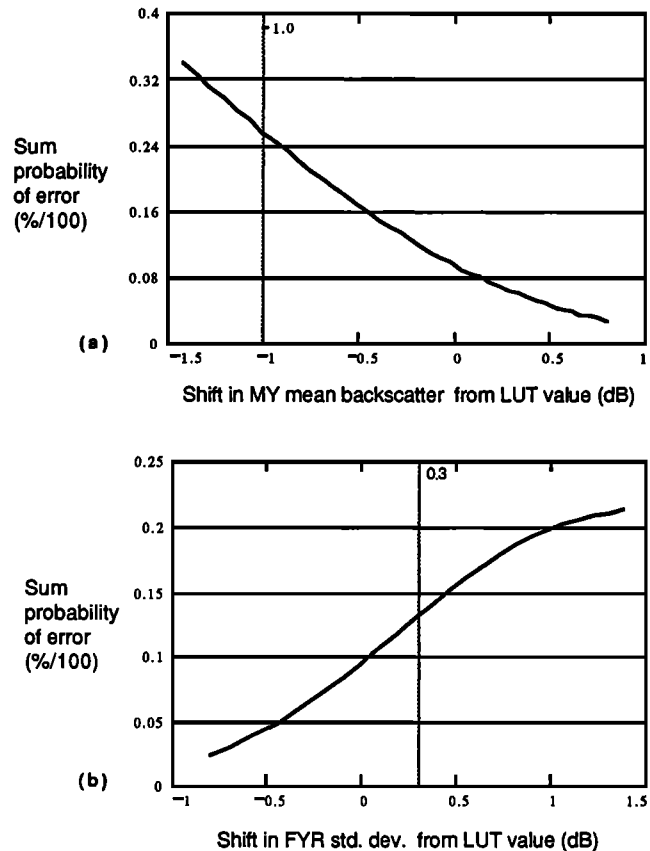


Figure 5. Theoretical error $P(\text{FYR}|\text{MY}) + P(\text{MY}|\text{FYR})$ due to (a) between-class and (b) within-class variation in backscatter signature. Vertical bars mark error at 1 standard deviation off the LUT values (see Table 3).

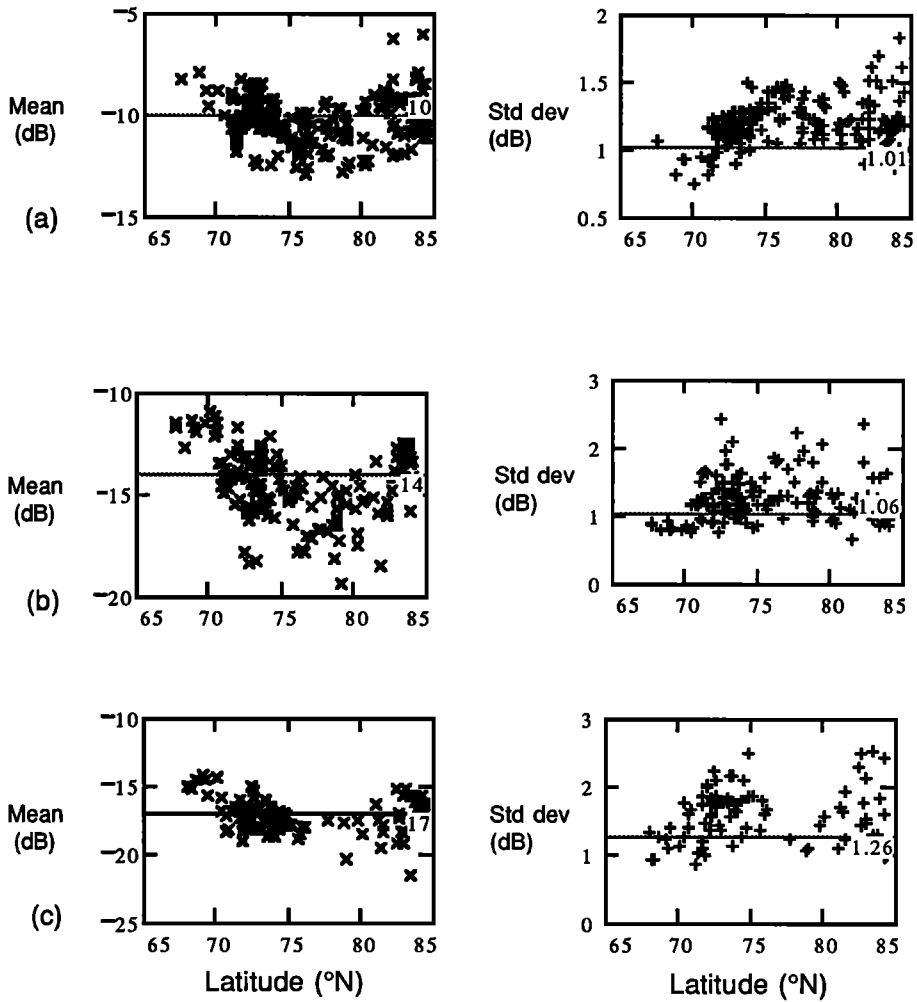


Figure 6. Backscatter statistics derived from training sets selected by the analyst as a function of latitude for (a) MY, (b) FYR, and (c) FYS ice.

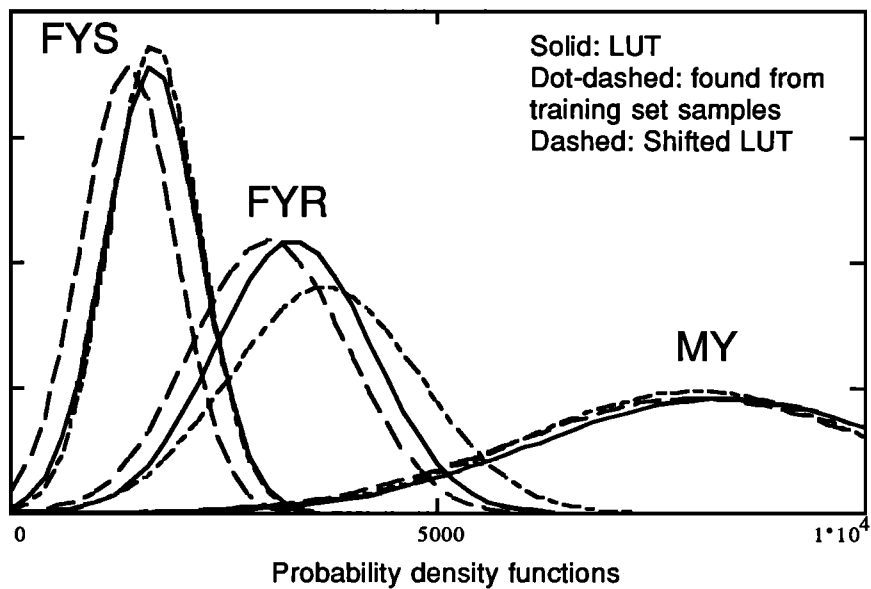


Figure 7. Backscatter distributions (plotted in intensity divided by a scale factor of 1.2×10^{-5}) from the LUT, from the averages of the training set samples (found distributions), and from the LUT shifted to match the mean found MY backscatter.

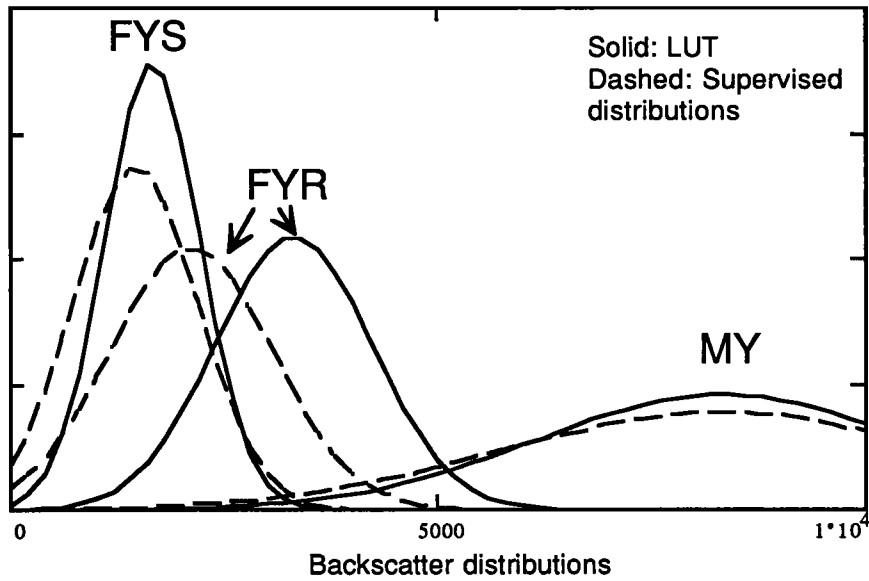


Figure 8. Backscatter distributions (plotted in intensity divided by a scale factor of 1.2×10^{-5}) derived from the average backscatter statistics of training sets used in the supervised classification of the image in Plate 1. The LUT distributions are also plotted.

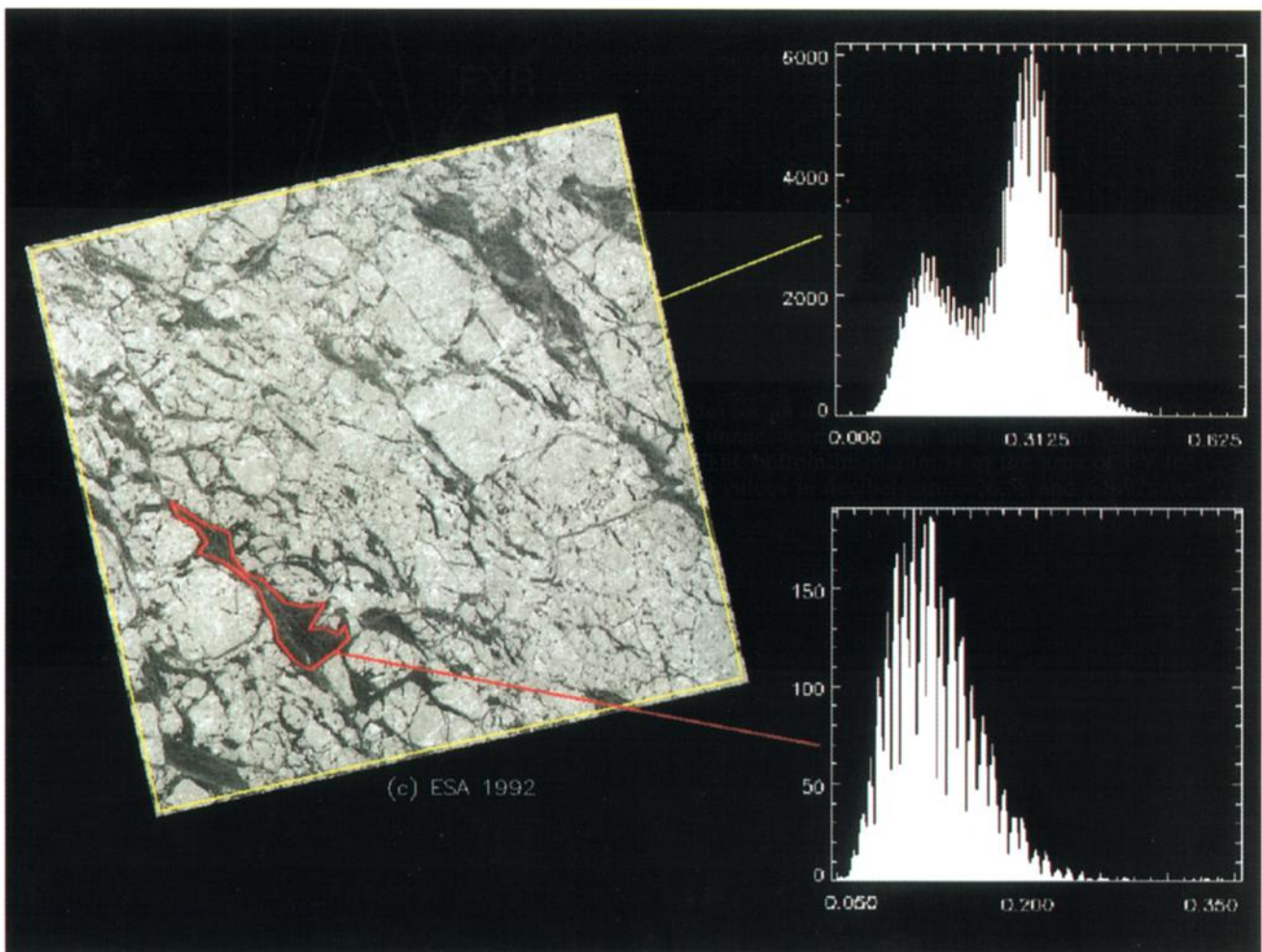


Plate 4. Histograms of calibrated pixel values (amplitude) for an image from the March 29, 1992, pass. The top histogram is of amplitude values for the entire image. The minimum and maximum values in decibels are -40.00 and -4.04 ; the mean is -11.30 dB. The bottom histogram is of the area of FY ice marked by the red line. Here the minimum and maximum values in decibels are -26.58 and -8.97 ; the mean is -17.71 dB. Copyright ESA 1992.

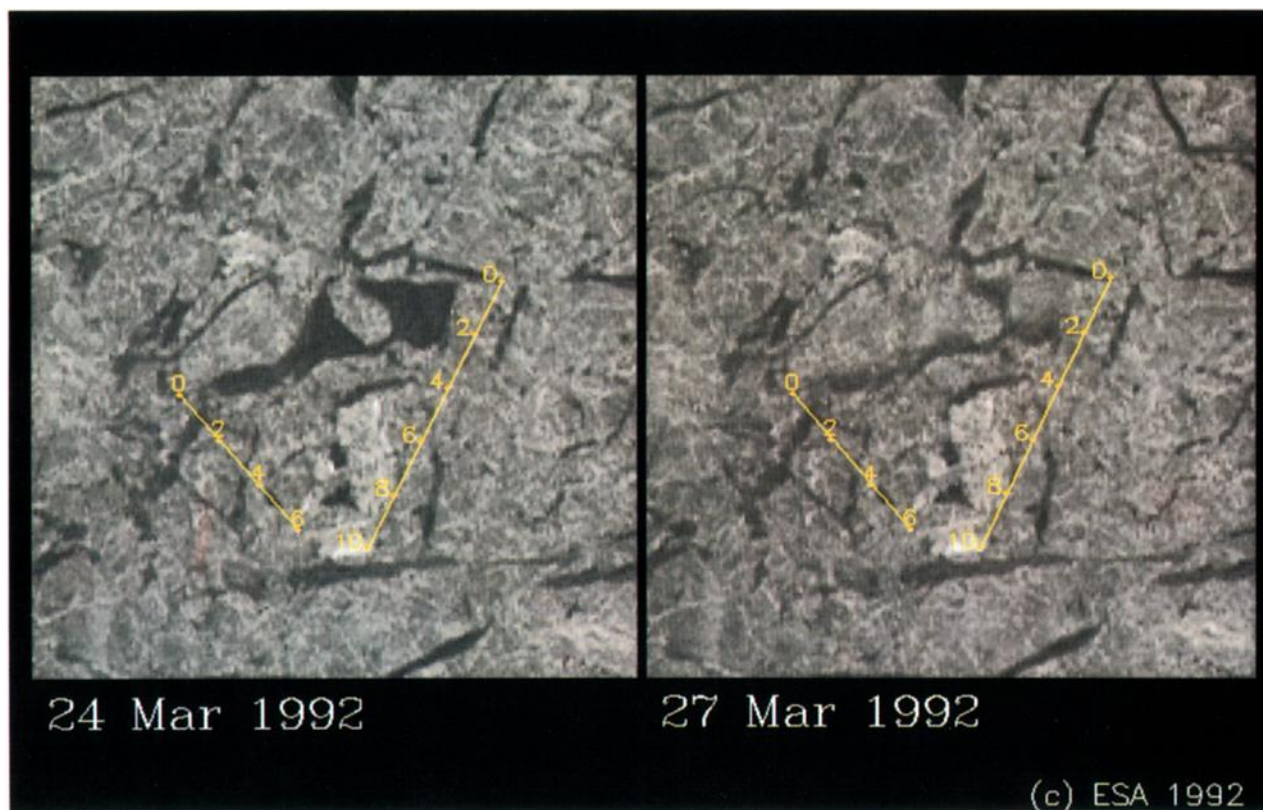


Plate 5. Some of the dark ice in the image at left has become indistinguishable on the basis of backscatter from adjacent MY ice, as shown in the image from 3 days later on the right. The yellow lines mark distance in kilometers to identical points on each image and indicate that the ice has not undergone any obvious deformation. The area of increased backscatter is unusual in that areas of new and young ice for which such a change is expected are generally linear in shape in this region and season. Copyright ESA 1992.

6.2. Separating Deformed From Undeformed Ice

The classifier's estimate of NI/OW concentration is known to be in error, at least some of the time, for the reasons discussed in section 4. More problematic is the issue of whether or not the classifier can distinguish two classes of FY ice consistently and of whether those classes correspond to identifiable geophysical characteristics of FY ice. For most images, two classes of FY ice (that is, of ice with backscatter lower than that of MY and higher than the noise floor but which, from contextual clues, does not appear to be new or young ice in a frozen lead) were obvious to the analyst performing supervised classification. The analyst called FYR ice that ice which was brighter overall, was heavily marked by a network of bright linear features suggesting ridges, or both. The analyst called FYS ice that ice which was of lower backscatter, with low apparent ridge density. Backscatter distributions of these two classes in a single image did not always approach the LUT distributions, however. Figure 8 shows LUT distributions with the distributions of FYR and FYS from manual analysis of the image in Plate 1. It is clear why the algorithm finds more FYS in this image than does the analyst.

The problem of choosing appropriate distributions for two FY types becomes clear when a histogram of image backscatter is displayed (Plate 4). The peaks for FY and MY ice are clearly separated. In separating the FY types, however, the algorithm is merely level slicing somewhere (determined by the LUT) along the FY peak. One possible classification

improvement, then, is to classify using ML iterative for good MY/FY classification and then attempt to separate FY ice into two classes if bimodal distributions are in evidence when local histograms are examined. This possibility has not been investigated. Plate 4 also shows the distribution of backscatter within an all-FY ice area.

6.3. Summary

Supervised classification is classification using a user-generated LUT, while classification by the algorithm uses an assumed LUT (shifted to account for the backscatter of MY ice in the image). If the backscatter distributions for the ice types are normal (and our analysis shows that they are), then the scatter of points in Figure 3 (quantified in Table 2) used to indicate error is the result of the difference between each image's backscatter distribution for each type and that of the assumed, unvarying LUT distributions. The varying means and standard deviations, from image to image, shift the position and overlap of the class distributions in a manner which results in the overall error rates shown by Figure 5. Of course, other factors besides natural within- and between-class variability contribute to class distributions which may be different than those of the LUT. The calibration could be wrong, but unless it is off by more than 2 dB this will not impair the performance of the algorithm owing to the sliding scale feature. The Isodata clustering routine could locate the position of the MY cluster inaccurately, resulting in an incorrect mean MY backscatter determination. The im-

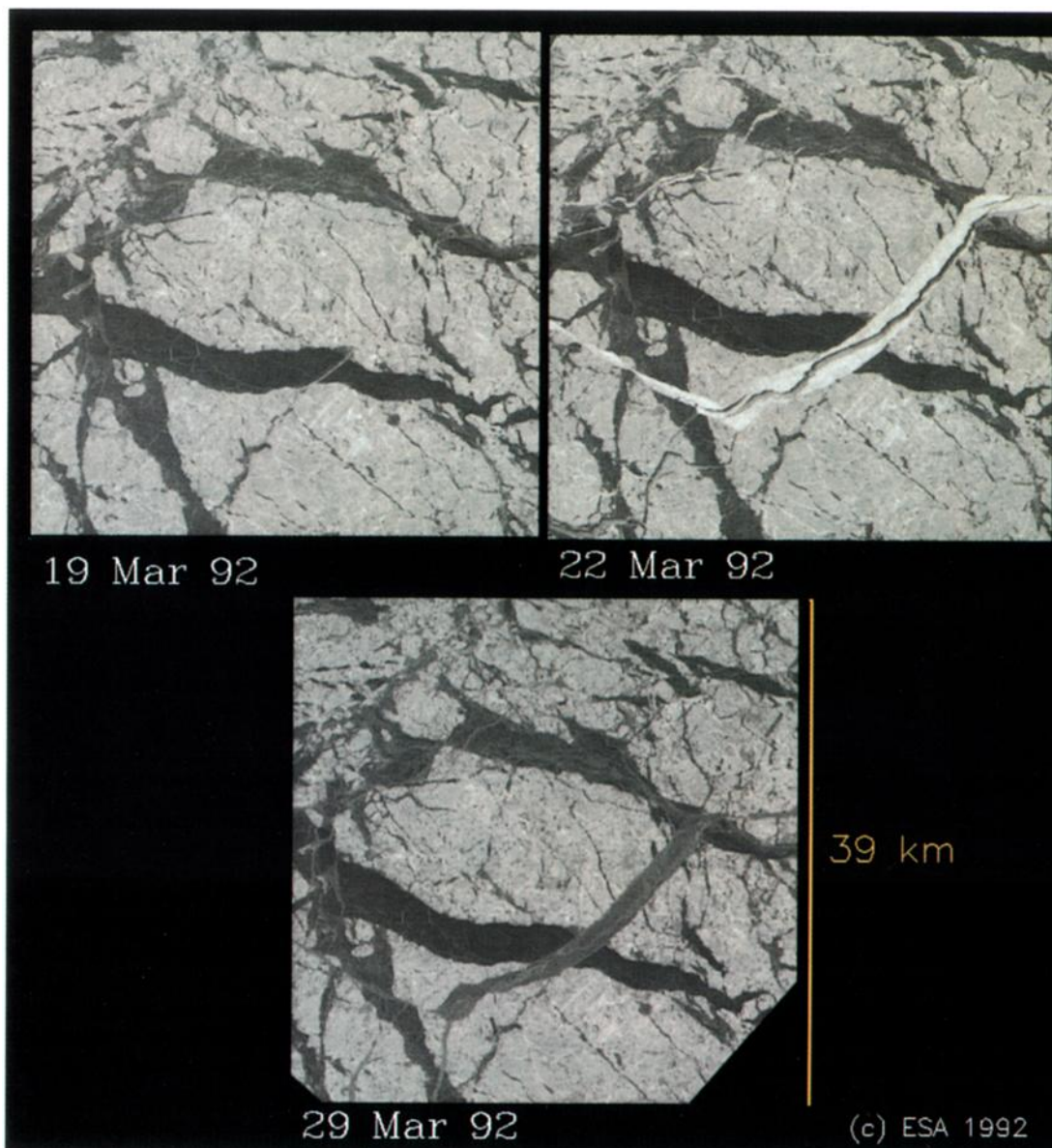


Plate 6. The image sequence shows an example of the change in backscatter which can occur as lead ice freezes. Because the lead ice in the lower image is only 10 days old, it must be young ice, yet its backscatter signature falls within that of FY ice. Copyright ESA 1992.

provement in the RMS difference of 1.1% between ML and ML iterative (which results in a more accurate determination of MY backscatter in the image by the clustering routine) is equivalent to a shift of less than 0.1 dB in the mean for MY ice. The difference between the MY cluster center found by the ML iterative version and the true center is likely to be even smaller than this. The order of this error is therefore likely to be small. While some of the discrepancy between algorithm and supervised classification is due to human inconsistency (about 2.8% for MY ice, equivalent to a change of about 0.15 dB from the MY value in the LUT), the majority of the approximately 6% discrepancy is due to between-class variability (as discussed in section 6.1). The width of the ice type class distributions remains fairly stable from image to image. The mean value for each class varies by a greater amount (see Table 3) and results in the between-

class variability from image to image that introduces most of the algorithm error.

7. Discussion and Conclusions

The ASF classifier performs well when compared with human-guided classification; other work on the variability of ice signatures [Kwok and Cunningham, 1994] indicates that the good MY/FY separation obtained for our 3-week data set should be characteristic for winter in the perennial ice zone of the Beaufort, Chukchi, and Central Arctic. With how much confidence, though, can geophysical ice types be assigned to the MY, FYR, FYS, and NI/OW types labeled by the classifier? Again, freezing ice and open water are known to have signatures which can be identical to MY ice. In the winter, away from the marginal ice zone, however, the

concentration of these types which can mimic MY is expected to be relatively low. Discriminating these types in the 250-m resolution data may be a problem of small spatial extent, leading to mixed pixels, as well as one of no distinct radiometric signature. There is also evidence that some deformed FY or younger ice may have a backscatter signature indistinguishable from MY at ERS 1 radar parameters [Rignot and Drinkwater, 1994]. If present in sufficient quantity, this ice could call into question the accuracy of MY estimates from ERS 1 SAR. On the other hand, if this FY ice appears like MY ice in the single-band radar data because it is sufficiently thick and desalinated, then for some applications it may not be necessary to distinguish it from true MY ice. Plate 5 may be an example of how younger types can mimic MY. Plate 5 shows an image sequence in which ice with backscatter of -19 dB gains 7 dB over 3 days. The cause of the change is unknown.

Further validation exercises are needed to establish how backscatter distributions correlate to ice types identified by thickness, age, or physical characteristics, such as salinity and surface roughness. Combining SAR with other satellite data may be useful for corroborating ice type estimates and for illuminating sources of error or variability in estimates from different sensors. Carsey [1985], for instance, used coincident Seasat SAR and passive microwave scanning multichannel microwave radiometer data to strengthen his conclusion that brightness temperature changes in the summer pack are due primarily to changes in surface conditions, rather than to changes in open water concentration. Since satellite SAR and satellite passive microwave data are the only sources of winter MY concentration estimates over much of the Arctic, a comparison of estimates from these sensors is essential. SAR MY estimates tend to be lower than special sensor microwave/imager (SSM/I) estimates [Fetterer et al., 1993]. A case study (incomplete at this time) shows that MY concentration from SSM/I and SAR differs by an amount that depends on geographic location but averages about 15%. Steffen et al. [1993] examined a winter ERS 1 SAR image coincident with Landsat thematic mapper data. While noting that gray ice and nilas are indistinguishable from FY ice in the SAR image, they suggested that combining SAR with Landsat data would allow robust classification. This sort of approach is necessary to resolve the question of how much new or young ice is being misclassified (by both supervised and algorithm classification) as FY or MY ice. The extent of the error would depend on how much divergence the ice has recently undergone and would therefore vary in time and space.

Combining sensor data is one approach to overcoming the limitations of single-channel data. Making use of temporal clues is another, although it is difficult to envision how this might be done automatically. Plate 6 shows how ice which is difficult to distinguish from FY or MY appears to be a form of younger ice when earlier (or later) imagery of the same ice is examined.

To summarize, there is a need to increase confidence in the ASF ice type product through additional validation and comparison work. On the basis of the work presented here we recommend that future GPS algorithm designs not attempt to distinguish two FY ice types and that alternative methods of finding the concentration of NI/OW be explored. With that stated, the growing ice type product archive at ASF, whether used (when large enough) as a climatology or

for a temporal sequence of ice conditions, is of great value for testing the results of air-ice-ocean dynamic and thermodynamic models with observations. The description of physical processes which go into a model can only be assumed correct if observations of mass balance (represented by the ice type maps or gridded concentration fields) are consistent with model predictions. For instance, if a model predicts more summer ice than the observations of MY at freeze-up show, then something is wrong. When combined with estimates of divergence (readily derived from SAR image sequences), ice type maps are an observational tool with which to explore the relative roles of heat flux and ice deformation in changing ice thickness distributions (see, for example, Thorndike [1992]). Any winter loss of MY ice must be accounted for by ridging or by export through the Fram Strait. Furthermore, the broad thickness classes implied by the FY/MY separation (corresponding roughly to less than and greater than 200 cm) are an improvement over the parameterization of a uniform ice cover often used in global circulation models. Thickness fields from ice prediction models should roughly correlate with contoured MY concentrations. Finally, ASF MY estimates are an independent data source for Kalman filtering or other methods of data blending in models (see Collins [1992] and Rothrock and Thomas [1992] for a discussion of data blending).

Acknowledgments. The authors wish to thank Tim Gremillion, Sverdrup Technology, for invaluable technical and programming help. This paper benefited greatly from the suggestions of two anonymous reviewers. The work of F. M. Fetterer and D. Gineris was sponsored by the Chief of Naval Operations under program element 603704N, Commander D. Markham, program manager.

References

- Alaska SAR Facility Prelaunch Science Working Team, Science plan for the Alaska SAR Facility Program, *Publ. 89-14*, Jet Propul. Lab., Pasadena, Calif., 1989.
- Carsey, F., Summer arctic sea ice character from satellite microwave data, *J. Geophys. Res.*, **90**(C3), 5015–5034, 1985.
- Carsey, F., Review and status of remote sensing of sea ice, *IEEE J. Oceanic. Eng.*, **OE-14**(2), 127–138, 1989.
- Carsey, F., K. Jezek, J. Miller, W. Weeks, and G. Weller, The Alaska synthetic aperture radar (SAR) facility project, *Eos Trans. AGU*, **68**, 593–596, 1987.
- Collins, M. J., Information fusion in sea ice remote sensing, in *Microwave Remote Sensing of Sea Ice*, *Geophys. Monogr. Ser.*, vol. 68, edited by F. Carsey, pp. 431–442, AGU, Washington, D. C., 1992.
- Cunningham, G., R. Kwok, and B. Holt, Preliminary results from the ASF/GPS ice classification algorithm, in Proceedings of the 1992 International Geoscience and Remote Sensing Symposium (IGARSS '92), *Publ. 92CH3041-1*, pp. 573–575, Inst. of Electr. and Electron. Eng., New York, 1992.
- Duda, R. O., and P. E. Hart, *Pattern Classification and Scene Analysis*, John Wiley, New York, 1973.
- European Space Agency, Proceedings of the First ERS-1 Symposium, Space at the Service of our Environment, *ESA SP-359*, 1993.
- Fatland, R., and A. Freeman, Calibration and change detection of ASF/ERS-1 SAR image data, in Proceedings of the 1992 International Geoscience and Remote Sensing Symposium (IGARSS '92), *Publ. 92CH3041-1*, pp. 1164–1166, Inst. of Electr. and Electron. Eng., New York, 1992.
- Fetterer, F., D. Gineris, and C. Johnson, Remote sensing aids in sea-ice analysis, *Eos Trans. AGU*, **74**(24), 265–268, 1993.
- Fily, M., and D. A. Rothrock, Opening and closing of sea ice leads: Digital measurements from synthetic aperture radar, *J. Geophys. Res.*, **95**(C1), 789–796, 1990.

- Gloerson, P., and W. J. Campbell, Recent variations in Arctic and Antarctic sea-ice covers, *Nature*, 325, 33–36, 1991.
- Kwok, R., and G. F. Cunningham, Backscatter characteristics of the winter sea ice cover in the Beaufort Sea, *J. Geophys. Res.*, 99(C4), 7787–7802, 1994.
- Kwok, R., E. Rignot, B. Holt, and R. Onstott, Identification of sea ice types in spaceborne synthetic aperture radar data, *J. Geophys. Res.*, 97(C2), 2391–2402, 1992.
- Onstott, R., SAR and scatterometer signatures of sea ice, in *Microwave Remote Sensing of Sea Ice*, *Geophys. Monogr. Ser.*, vol. 68, edited by F. Carsey, pp. 73–104, AGU, Washington, D. C., 1992.
- Rignot, E., and M. R. Drinkwater, Winter sea ice mapping from multi-parameter synthetic aperture radar, *J. Glaciol.*, 40(134), 31–45, 1994.
- Rothrock, D. A., and D. R. Thomas, The Arctic ocean multi-year ice balance, 1979–82, *Ann. Glaciol.*, 14, 252–255, 1990.
- Rothrock, D. A., and D. R. Thomas, Ice modeling and data assimilation with the Kalman smoother, in *Microwave Remote Sensing of Sea Ice*, *Geophys. Monogr. Ser.*, vol. 68, edited by F. Carsey, pp. 405–418, AGU, Washington, D. C., 1992.
- Steffen, K., J. Heinrichs, J. Maslanik, and J. Key, Sea ice feature and type identification in merged ERS-1 SAR and Landsat Thematic Mapper imagery, in *Proceedings of the First ERS-1 Symposium, Space at the Service of our Environment*, Eur. Space Agency *Spec. Publ.*, ESA SP-359, 361–365, 1993.
- Strahler, A. H., The use of prior probabilities in maximum likelihood classification of remotely sensed data, *Remote Sens. Environ.*, 10(2), 135–163, 1980.
- Thorndike, A. S., Estimates of sea ice thickness distribution using observations and theory, *J. Geophys. Res.*, 97(C8), 12,601–12,605, 1992.
-
- F. M. Fetterer, Naval Research Laboratory, Remote Sensing Applications Branch, Stennis Space Center, MS 39529.
D. Gineris, Sverdrup Technology, Stennis Space Center, MS 39529.
- R. Kwok, Jet Propulsion Laboratory, California Institute of Technology, 4800 Oak Grove Drive, Pasadena, CA 91109.

(Received November 12, 1993; revised July 6, 1994; accepted July 14, 1994.)